Ultrahigh Gain, Low Noise, Ultraviolet Photodetectors with Highly Aligned Organic Crystals

*Yongbo Yuan and Jinsong Huang**

Organic semiconductor materials including small molecules and polymers have potential in many applications due to their highly tailorable optoelectronic properties, good flexibility, and low cost.[1–3] Here we show that an organic phototransistor using highly aligned 2,7-dioctyl[1] benzothieno,[1,2b,3] benzothiophene (C8-BTBT) polycrystalline films as the photoactive layer has a high gain of above 10^7 under weak ultraviolet (UV) light. The gain reaches the parity of photomultiplier tubes (PMTs) but with a driving voltage of tens of times lower than that of PMTs.[4] In addition, the application of photovoltaic-mode operation of the organic phototransistor gives rise to an extremely low noise in the order of subnanoampere. The very high gain can be explained by the high hole mobility and efficient electron trapping capability of C8-BTBT, enhanced dissociation of electron–hole (e–h) pairs and reduced e–h recombination by the applied gate field. Both single-pixel photodetector and large-area photodetector arrays have been demonstrated which are integrated onto silicon substrates.

Photodetectors with high sensitivity in UV range but negligible response in visible range is desired in many civilian and military applications, such as health care,[5] chemical sensing,[6] air pollutants monitoring,[7] combustion and flame detection,[8] missile warning,[9] and radiation detection.[10] PMTs, invented in 1935 by R.C.A. Radiotron Company, Inc., remain among the oldest tools still in widespread use in weak light detection due to their excellent detectivity, which combines a high gain (defined by the collected charges per absorbed photon) of 10^5–10^7 and very low noise in the range of 100 pA at room temperature.[4,11] However, the applications of PMTs are limited due to their high cost and some other intrinsic disadvantages/limitations, such as high working voltage (>1000 V), fragile glass-tube structure, susceptibility to magnetic field, and complex cooling sytem. [4] Therefore, it is urgent to develop compact and robust solid-state photodetectors with high sensitivity, good flexibility, and low cost.[12–16]

In past decades, organic semiconductors have received incredible success in many applications, such as organic light-emitting diodes (OLEDs),[1] organic photovoltaics (OPVs),[2] and organic field-effect transistors (OFETs)[3] due to their versatile molecular structures and hence tailorable optoelectronic properties, including bandgap, absorption, carrier mobility, trap densities, charge recombination rate, etc.[17] Besides, organic materials can be conveniently deposited by low temperature solution methods, making them quite promising in the mass production of optoelectronic devices with low cost.[18] Organic semiconductors are appealing light detection materials due to their much stronger light absorption than most inorganic counterparts.[19,20] Nevertheless, the low carrier mobility of organic semiconductors, which is usually in a range of 10^{-6}–1.0 $cm^2\ V^{-1}\ s^{-1}$, limits their application for high performance photodetectors. Encouragingly, we recently demonstrated that C8-BTBT polycrystalline films fabricated by an "off-centre spin-coating" method can have an ultrahigh average hole carrier mobility of 25 $cm^2\ V^{-1}\ s^{-1}$.[21] This high carrier mobility provides a platform for exploring high performance organic photodetectors. In this study, we reported highly sensitive phototransistors with the highly aligned C8-BTBT polycrystalline films as the active layers.

The organic transistor we used here has a top-contacted bottom-gated structure (**Figure 1**a). The highly aligned C8-BTBT polycrystalline films were casted from a blended solution of C8-BTBT and polystyrene (PS) using the "off-centre spin-coating" method.[21] The molecular structures of C8-BTBT and PS are shown in Figure 1a. The C8-BTBT films had an edge-on alignment on the substrate and form monoclinic crystal structure. The in-plane stacking of the C8-BTBT molecules is illustrated in Figure 1a. Highly doped silicon wafer with a 300 nm SiO_2 layer was used as the substrate and gate electrode, which also demonstrates the direct integration of the organic phototransistors with silicon chips. The dielectric layer contains the 300 nm thermally grown SiO_2 layer and a 330 nm crosslinked poly(4-vinylphenol) (PVP) layer,[22] which has a total specific capacitance of 6×10^{-5} F m^{-2}. We used thick dielectric layer because it can cause smaller leakage current and a larger threshold voltage shift that is needed for sensitive photodetection reported here (see Figure S1 in the Supporting Information).[23]

The C8-BTBT films fabricated on crosslinked PVP surface had a very high degree of crystallinity and crystal alignment, as evidenced by the clear anisotropic absorption spectra in the wavelength range of 295–375 nm (Figure 1b). The strong dependence of the absorption with the polarization of the incident light beam indicates the presence of highly oriented C8-BTBT molecules in a macroscopic scale, since the light spot in the measurement was >3 mm^2.[21,24] The presence of three absorption peaks (e.g., 360, 342, and 325 nm) is due to the excitation of electrons from ground state into different vibrational states with an energy step of 0.19 eV.[25] For the C8-BTBT film with a thickness of 15 nm, the absorption at 354 nm is 15% or 6% when the electrical field (E) of polarized light is parallel or perpendicular to the (100) direction of the C8-BTBT crystals (Figure 1b), respectively, giving an average absorption of around 10% for nonpolarized light.

Dr. Y. Yuan, Prof. J. Huang
Department of Mechanical and Materials Engineering
University of Nebraska-Lincoln
Lincoln, NE 68588-0656, USA
E-mail: jhuang2@unl.edu

DOI: 10.1002/adom.201500560

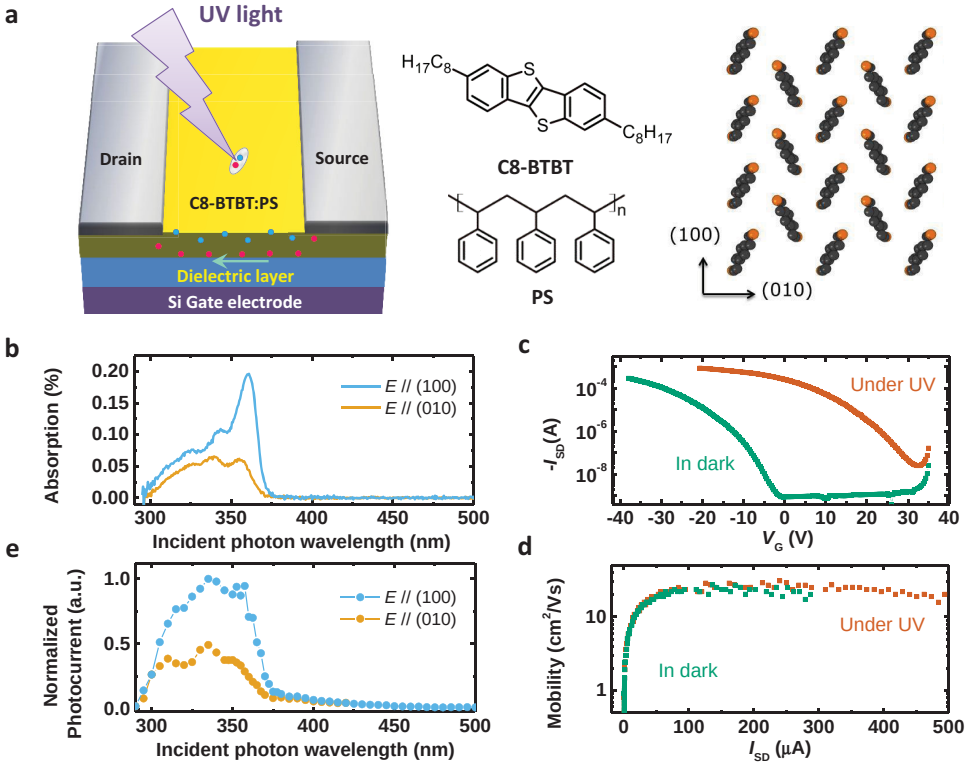

Figure 1. Efficient UV phototransistor detector with highly aligned C8-BTBT crystal film as the photoactive layer. a) Schematics of the organic phototransistor integrated on Si substrate, where the molecular structures of the C8-BTBT and polystyrene (PS) are shown. The right side illustrates the in-plane stacking of C8-BTBT molecules; b) anisotropic polarized-absorption spectrum of the highly aligned C8-BTBT crystal film, where the light electrical field is along the (100) direction or (010) direction of the C8-BTBT crystal, respectively; c) I_{SD}–V_G curve of the C8-BTBT phototransistor in dark condition and under UV light with an intensity of 14 μW cm^{-2}, respectively, where the V_{SD} is −30 V; d) calculated mobility from the slope of the transfer curves, where the corresponding I_{SD} is shown in the Figure 1c; and e) normalized photocurrent response spectrum of the phototransistor, where the electrical field of the incident monochromic light is along the (100) direction or (010) direction of the C8-BTBT crystal, respectively.

The threshold voltages of these transistors change under illumination, as shown by the channel-current (I_{SD}) versus gate-voltage (V_G) curve in Figure 1c. This feature allows the operation of this type of transistor as photodetector with both high signal and low noise by monitoring the I_{SD} change at the threshold gate bias (V_{th}) in the dark. The noise current of the photodetector in the dark is thus very small, because the transistor is turned-off. The signal of the photodetector is large because of both the right- and upshift of the transfer curve. Such a phototransistor is very sensitive because of the largest signal/noise ratio which is the figure of merit for a photodetector. As shown in Figure 1c, the V_{th} for the C8-BTBT transistor in the dark is around –1.5 V. This V_{th} shifted positively to be around 30 V when the channel was illuminated under 14 μW cm^{-2} UV light, which corresponds to a typical photovoltaic operation mode in the a phototransistor.[26,27] At the gate bias of –1.5 V, a weak UV light of 14 μW cm^{-2} caused a large ΔI_{SD} of 0.31 mA, corresponding to a huge responsivity of 2.2×10^4 A W^{-1} (the channel area was 0.1 mm^2) and a signal/noise ratio of >10^5. At a more negative gate bias of –20 V, the responsivity further increased by twofolds, which can be explained by the increased charge separation and charge extraction by the larger gate bias.[26] However, the higher responsivity obtained at –20 V was accompanied with a dramatically increased noise current by 10^4 times, which reduced the signal/noise ratio to ≈50. This demonstrates the operation of these phototransistors at V_{th}.

The hole mobility calculated from the slope of the transfer curve ($I_{SD}^{1/2}$–V_G), is over 20 cm^2 V^{-1} s^{-1} in an I_{SD} region of 50 μA ≈300 μA (Figure 1d). Apparently, the UV illumination does not impact on the hole mobility of the C8-BTBT despite of the dramatic V_{th} shift. The obtained responsivity spectrum (Figure 1e) has same peak positions with the absorption spectrum (Figure 1b), indicating the C8-BTBT film is the photoactive layer. In the responsivity spectrum, the relative intensity of each peak is different from that of the absorption spectrum, which might be due to a larger exciton dissociation efficiency (η_{dis}) for the e–h pairs generated by higher energy UV photons, e.g., at the 2nd and 3rd absorption peak (Figure S2, Supporting Information). Similar increased dissociation of e–h pairs has been observed in pristine C_{60} crystal film with strong intermolecular electron cloud overlapping.[28] The weak binding between photogenerated holes and electrons is consistent with the observed delocalization of holes in the C8-BTBT crystal, which results in a slow recombination between e–h pairs and thus large photocurrent under illumination.[29]

The photodetectors were characterized at different incident light intensity from 14 pW cm^{-2} to 14 μW cm^{-2} (**Figure 2**a,b) to find out its linear response. The ΔV_{th} and photocurrent (I_{light} – I_{dark}) obtained at the gate voltage of –1.5 V is plotted

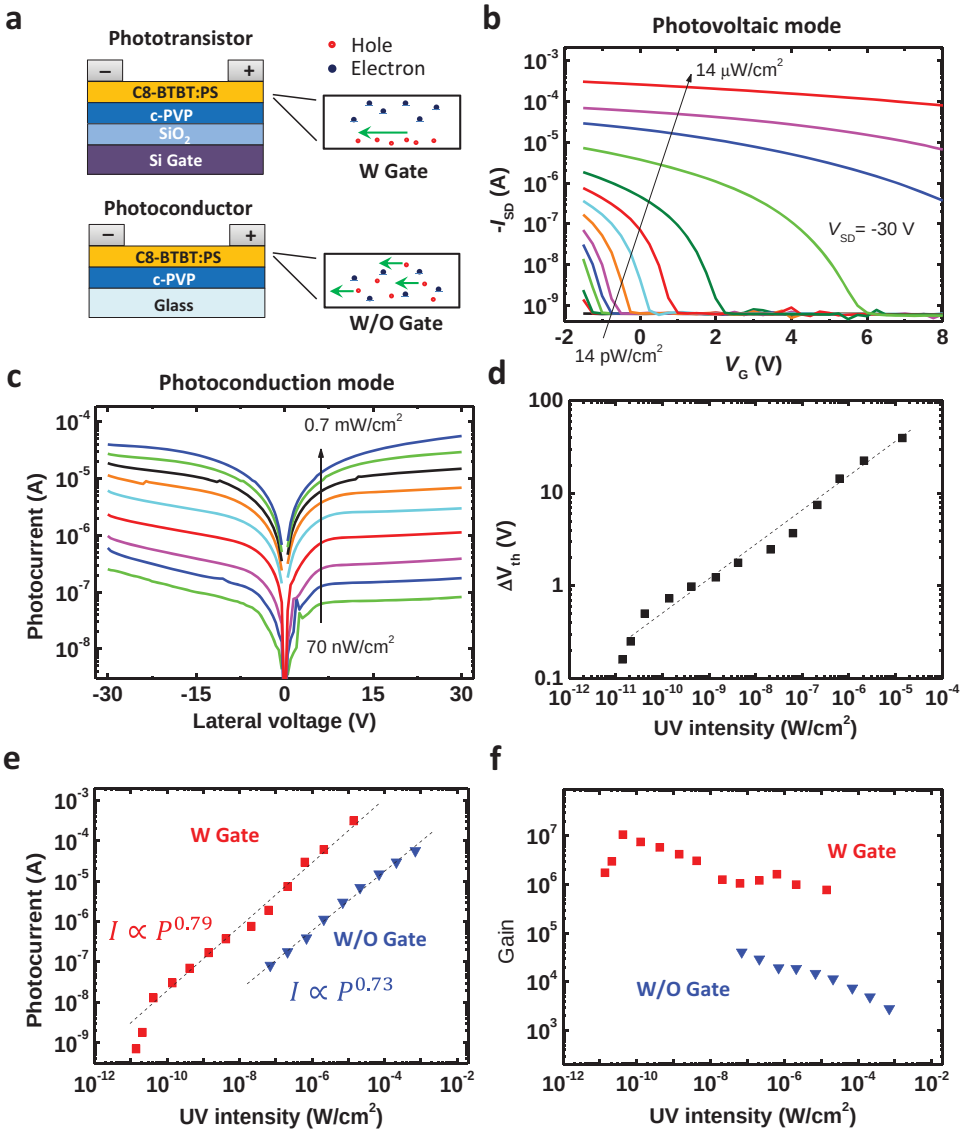

Figure 2. Ultrahigh detecting gain obtained by C8-BTBT phototransistor and its origins. a) Structures of the C8-BTBT phototransistor and lateral photoconductor, respectively, where the C8-BTBT crystal film was fabricated on PVP surface in both case; b) $I_{SD} - V_G$ curves of the C8-BTBT phototransistor under UV illumination with light intensities varied from 14 pW cm^{-2} to 14 μW cm^{-2}; c) photocurrent ($|I_{light} - I_{dark}|$) of the lateral photoconductor under UV illumination with light intensities varied from 70 nW cm^{-2} to 0.7 mW cm^{-2}; d) dependence of the threshold voltage shift (ΔV_t) on the incident UV light intensity; e), dependence of the photocurrent ($I_{light} - I_{dark}$) of the phototransistor (red curve, obtained at $V_G = -1.5$ V) and photoconductor (blue curve) on light intensity; and f) comparison of the detecting gain of C8-BTBT phototransistor (red curve) and C8-BTBT photoconductor (blue curve).

in Figure 2d,e, respectively, with respect to the incident light intensity. The logarithm of ΔV_{th} has a linear relationship with the logarithm of light intensity (i.e., $\Delta V_{th} = P^{0.36}$, Figure 2d). The ΔV_{th} did not follow the common empirical formula of $\Delta V_{th} \propto \log P$.[30] This might be related to a small recombination rate between the delocalized holes and trapped electrons, so that the increase of the ΔV_{th} do not saturate for the transistor under higher light intensity. Meanwhile, there is also a linear relationship between logarithm of the photocurrent and logarithm of the light intensity (i.e., $\Delta I_{SD} = P^{0.79}$) in a light intensity range of from 42 pW cm^{-2} to 14 μW cm^{-2}. This ΔI_{SD}–P relationship can be explained by the relationship between the ΔV_{th} and light intensity. The saturation channel current of a transistor is determined by $I_{SD} \propto (V_G - V_{th})^2$, therefore, the channel current should be proportional to the square of the ΔV_{th}.[31] The obtained $\Delta I_{SD} \propto \Delta V_{th}^{2.2} \propto P^{0.79}$ in Figure 2e is thus consistent. The photocurrent starts to diverge from the linear relationship when the light is weaker than 42 pW cm^{-2}. The lowest detectable light intensity, i.e., noise equivalent power (NEP), was 14 pW cm^{-2}.

The photodetector gain (G), defined by the collected charge number per absorbed photon by the C8-BTBT layer, was summarized in Figure 2f. Strikingly, a maximum gain of 1.1×10^7 (corresponding to a responsivity of 3.1×10^5 A W^{-1}) was obtained at a very weak light intensity of 42 pW cm^{-2}, which is the highest achieved gain by

organic photodetectors so far.[26,27,32] In order to find out the origins of the ultrahigh gain of our phototransistors, control C8-BTBT photoconductors have been fabricated on glass substrate without a gate electrode beneath the C8-BTBT/PVP layer (Figure 2a). These lateral photoconductors have same working area and electrode geometry with that of the phototransistors. To ensure same high crystallinity and alignment of the C8-BTBT polycrystalline film, the glass substrate was covered by a same cross-linked PVP layer. Figure 2c shows the photocurrent-voltage curves of a C8-BTBT photoconductor at varied UV intensity from 70 nW cm^{-2} to 0.7 mW cm^{-2}. This photoconductor did not show clear photocurrent signal at light intensity weaker than 70 nW cm^{-2} because of its relative large dark current of 300 nA (see Figure S3 in the Supporting Information). The photocurrent ($I_{light} - I_{dark}$) of the photoconductor also shows a power relationship with light intensity (Figure 2e). The highest internal gain of the photoconductor was 4×10^4 at an UV light intensity of 70 nW cm^{-2} (Figure 2f), which is remarkably high as compared to many other thin film photoconductors, but is still around 50 times lower than that of the phototransistor under same light intensities.[15,33] This indicates the amplification of the transistor structure contributes to the observed high gain. In a photoconductor device, G is determined by the transit time (τ_{tran}) and the carrier charge recombination lifetime (τ_r) [13,34]

$$G = \eta_{dis} \times (\tau_r / \tau_{tran}) \quad (1)$$

where $\tau_{tran} = d^2 / \mu V$ is determined by the electrode spacing (d), hole carrier mobility (μ) and the applied bias (V). The high gain obtained in the C8-BTBT photoconductor is benefited from the large hole mobility in the highly aligned C8-BTBT polycrystalline films. Besides, it also indicates that the polycrystalline C8-BTBT film has sufficient long hole recombination lifetime. The low limit hole recombination time is estimated to be on a level of 0.1 s if assuming the hole mobility in C8-BTBT photoconductor is as high as that in C8-BTBT transistor (20 cm^2 V^{-1} s^{-1}) and the η_{dis} is 100%. This long recombination lifetime might be related to the weak binding between e–h pairs.[12,13] It also indicates an efficient electron trapping capability of the C8-BTBT film, otherwise those electrons would be swept out of the film by the lateral electrical field.

The maximum gain obtained in the phototransistor is over 200 times higher than that in the photoconductor (Figure 2f). We speculate three reasons for this dramatic performance enhancement: (1) the dissociation of the photogenerated e–h pairs (η_{dis}) is more efficient in phototransistor due to the presence of a gate field in the order of 1 MV m^{-1};[26] (2) the average hole mobility in transistor structure (20 cm^2 V^{-1} s^{-1}) should be higher than that in the photoconductor because more traps were filled by the high density of hole carriers.[35] This is because most of the holes in the transistor transport in a narrow region affinity to the PVP/C8-BTBT interface within only few monolayers;[36] and (3) the recombination between transporting holes and trapped electrons is reduced in the transistor. The confinement of holes in a narrow region also leads to a spatial separation between the transporting holes and the trapped electrons, which reduces their recombination, as illustrated in Figure 2a. This reduced e–h recombination was proved by the observed slower photocurrent decay rate in the C8-BTBT phototransistor (Figure S4, Supporting Information).

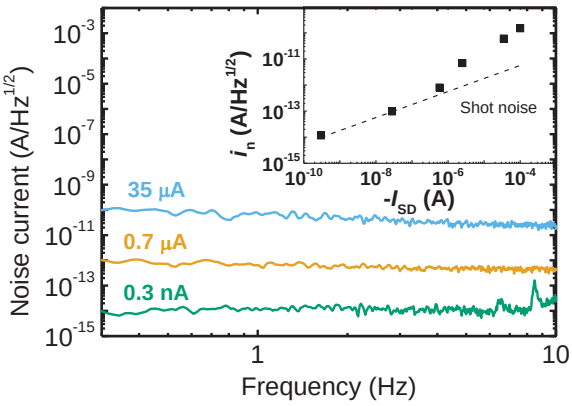

Figure 3. Noise current in C8-BTBT phototransistor. Noise current spectrum of the C8-BTBT phototransistor at different channel current states, where the channel current is ≈0.3 nA when the phototransistor was turned off. Inset shows the noise current at 1 Hz against to the channel current, indicating the low noise character of the highly aligned C8-BTBT polycrystalline film.

It is noted although a high gain of 10^8 have been observed in phototransistors with graphene channel, the high gain was obtained under high light intensity >10 nW cm^{-2}, which is over hundreds of times stronger than the UV light intensity reported here.[20,37] A high gain is preferred for a photodetector under weak light, because the photocurrent is large under strong light, anyway. Since the detection of weak light is much influenced by the fluctuation of the dark current, reducing the dark current is crucial in all types of photodetectors.[16] As compared to graphene phototransistors, a main advantage of the C8-BTBT phototransistors is that the device noise current can be completely turned off in the dark, which is not achievable for graphene transistors. The much lower dark current in C8-BTBT phototransistor detector than graphene phototransistors should also be ascribed to the much lower noise factor in C8-BTBT (see Figure S5 in the Supporting Information). **Figure 3** shows the measured noise spectrum of the C8-BTBT phototransistors with varied dark current. When the transistor is at the "off" state ($V_g > V_{th}$, $I_{SD} \approx 0.3$ nA), the noise is at a very low level of 1×10^{-14} A Hz$^{-1/2}$ at 0.1 Hz – 10 Hz, which is mainly determined by the shot noise floor (inset of Figure 3). At a higher dark current of 100 nA–100 μA, the noise spectrum is dominated by $1/f$ noise (see Figure S5a in the Supporting Information). According to Hooge's empirical equation,[38] the noise power (S_I) is inversely proportional to the frequency (f): $S_I / I_{SD}^2 = \alpha / Nf$, where α is the Hooge's parameter and N is the total number of free charge carriers. The parameter α of C8-BTBT varied in a range of 10^{-4}–10^{-2}, which is comparable to that of the Si metal-oxide-semiconductor FETs (10^{-3}).[39] The small α may be explained by the low concentration of hole traps in the C8-BTBT film or/and at the PVP surface.[21] The measured specific noise factor η, defined as $\eta = S_I L^2 / I_{SD}^2 R$, where L is the channel length and R is the channel resistance, has a small value of ≈10^{-16} μm^2 Ω^{-1}, when the transistor is in a high resistance state ($R/L > 10^6$ Ω μm^{-1}; see Figure S5b in the

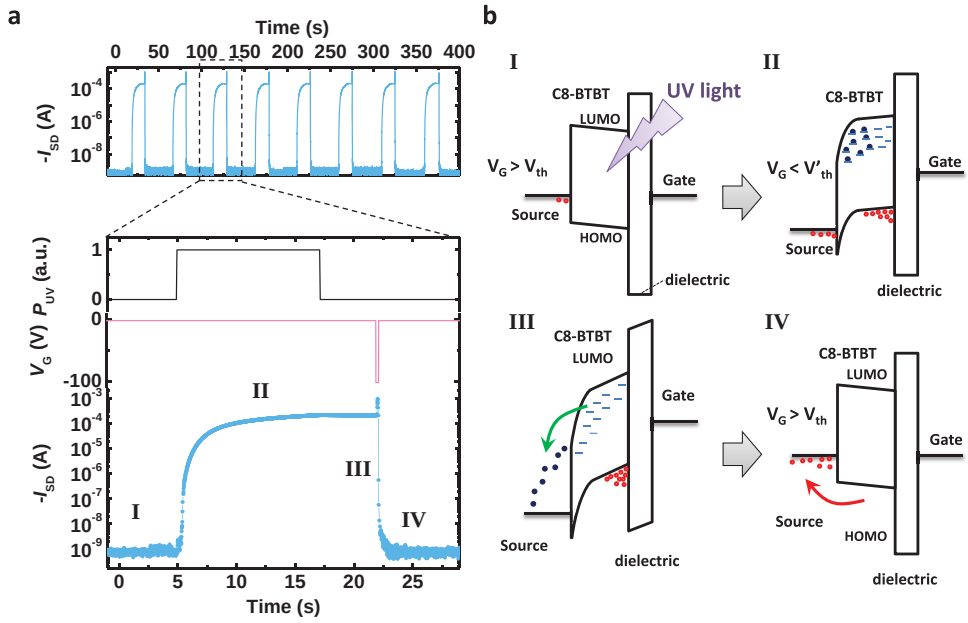

Figure 4. Detecting and resetting process of C8-BTBT phototransistor. a) Response of the channel current to repeated light illumination (14 μW cm^{-2}) and resetting electrical pulses; b) energy diagrams of the C8-BTBT phototransistor under dark condition (I), after UV illumination (II), under a large negative gate voltage pulse (resetting, III), and after electrical resetting (IV).

Supporting Information). It is thousands of times smaller than the reported noise factor of graphene (≈5×10^{-13} μm^2 Ω^{-1}).[40]

The current output of the C8-BTBT phototransistor under repeated light pulse and resetting electrical pulses is shown in **Figure 4**a, where the corresponding energy diagram was illustrated in Figure 4b. In the dark (i.e., the first 0–5 s, marked as stage "I"), the transistor is turned off and there is no free charges in the channel (Figure 4b, I). When the C8-BTBT was illuminated by weak UV light of 14 μW cm^{-2}, the channel current increased by around six orders of magnitude ("II" stage) due to the generation of trapped electrons and transporting holes (Figure 4b, II). Here the dissociation of the photogenerated e–h pair is benefited from the strong intermolecular electron cloud overlapping between C8-BTBT molecules and hence the weak binding between the electrons and holes, as has been discussed above. Due to the strong electron trapping effect of C8-BTBT film, the trapped electrons remain in C8-BTBT layer at the relative small gate bias of –2 V. Before recombining with the trapped electrons, the photogenerated hole carriers could drift through the channel region for 10^6 times. Considering the high mobility value of 20 cm^2 V^{-1} s^{-1}, the transit time for the hole drifting through the 100 μm channel is around 5 μs. The device response time is estimated to be 5 s based on the high gain of around 10^6. This estimation is consisting with the device turn-on time shown in Figure 4a (about 12 s, a longer time is needed because the η_{dis} in Equation (1) is actually less than 100%). After the illumination, due to the strong electron trapping capability of the C8-BTBT crystal film, a large negative gate bias (–102 V in this case) is needed to detrap the electrons out of the channel and reset the phototransistor (Figure 4b, III). The function of the large negative gate bias is to draw the trapped electrons out of the C8-BTBT film. Without resetting the gate voltage, it takes hundreds of seconds for the phototransistor returns to "off" state through the e–h recombination process (Figure S4, Supporting Information), while a short voltage pulse of 0.1 s is sufficient to remove the trapped electrons if a large gate voltage of –102 V was used. When the gate bias resumed from –102 V to –2 V, the transistor switched back to the "off" state (Figure 4b, IV). This kind of organic photodetector can have reasonable stability under UV illumination since organic molecule with similar structure shows no degradation after UV illumination for 200 h.[12]

The small pixel photodetectors demonstrated here can be easily integrated due to the simple device structure. For some application, a large photodetection area is needed. Here we demonstrate that large area by combining an array of phototransistors, with a maximum detecting area of up to 3.6 mm^2, which was realized by using interdigitated source and drain electrodes (**Figure 5**a). Both the dark current and the photocurrent of these array devices increased linearly with the detecting area (Figure 5b; Figure S6, Supporting Information). The photocurrent for device with large active area of 3.6 mm^2 is 32 mA at a light intensity of 14 μW cm^{-2}, which is huge as compared to commercial Si diodes (Hamamatsu S2387). At a same light intensity, the commercial Si diode with a larger working area of 10 mm^2 has an output photocurrent of only 100 nA due to the absence of a gain. It turns out that these C8-BTBT phototransistors do not loss their high gain (2.2×10^6–2.6×10^6) and on/off ratio (1.5×10^6–3.3×10^6) when the detecting area increased from 0.05 to 3.6 mm^2. The retained high gain and on/off ratio at large area indicates the excellent uniformity of the device performance in the same array. In our previous study, it has been proved that the C8-BTBT crystal has balanced hole mobility along difference directions despite of the local crystal orientation and channel direction.[21] We believe the isotropic hole mobility property, in addition to the uniform aligned C8-BTBT

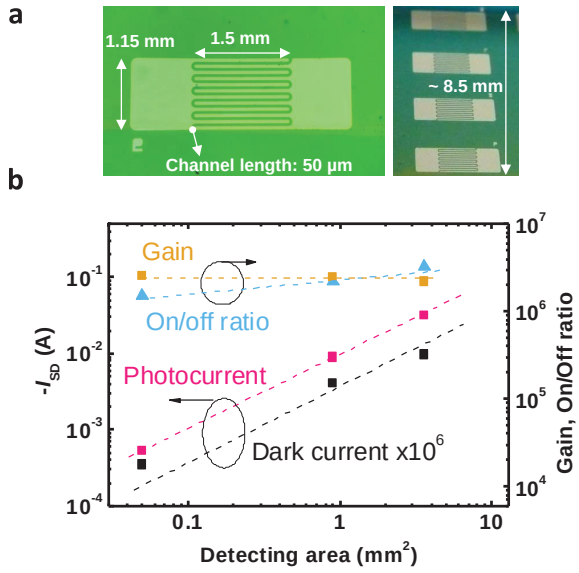

Figure 5. High gain C8-BTBT phototransistor with enlarged working area. a) Photos of the C8-BTBT phototransistors with interdigitated source and drain electrodes, where the channel length is 50 μm and the channel width is 18 mm. The right photo shows a detector array consisted of four C8-BTBT phototransistors in an area of 3.5 × 8.5 mm^2; b) photocurrent, dark current and on/off ratio of the C8-BTBT phototransistor with different working area, demonstrating the high detecting gain at a large working area of 3.6 mm^2.

films over a large area, contributes to the photodetector performance uniformity.

In summary, C8-BTBT polycrystalline films were found both a good hole transport material and electron trapping material. By using phototransistor with highly aligned C8-BTBT as the photoactive layer, an ultrahigh gain of 1.1×10^7 has been demonstrated at a weak light of 42 pW cm^{-2}, which is the highest value ever achieved with organic materials. The C8-BTBT phototransistor has much lower dark current and noise as compared to other type of high gain detector based on graphene. By simply depositing different electrode patterns on the C8-BTBT active layer, phototransistors with both miniature single pixel (0.05 mm^2) and large area photodetector arrays (3.6 mm^2) have been demonstrated without loss of sensitivity.

Experimental Section

Device Fabrication: For the phototransistor, highly doped silicon (Si) wafers with 300 nm thick thermally grown Si oxide (SiO_2) layer was used as the gate electrode and dielectric layer, respectively. For photoconductor, glass was used as the substrate. After being treated by UV-ozone, these substrates were covered by a cross-linkable PVP dielectric layer according to literature procedures. Here 4,4′-(hexafluoroisopropylidene)diphthalic anhydride (HDA) was used as the cross linker. The PVP:HDA blend (10:1 by wt) was dissolved in propylene glycol monomethyl ether acetate to form a solution with concentration of 100 mg ml^{-1}. The PVP:HDA blend was spin coated on SiO_2 surface at 4000 rpm for 40 s and then cured at 100 °C for 60 min to form a crosslinked PVP layer with a thickness of ≈330 nm. The organic semiconductor films were fabricated on PVP:HDA surface from a 5 mg ml^{-1} C8-BTBT:PS (95:5 wt%) solution in DCB via an established off-centre spin-coating method in an nitrogen atmosphere. The Si or glass substrate was placed with its centre away from the rotation axis of the spin-coater at a distance of 20–40 mm. During the off-centre spin-coating process, the spin speed was gradually increased to 2700 rpm. The resulted film is around 15 nm. Finally, silver (Ag) electrodes were thermally evaporated on C8-BTBT top through a Si shadow mask with a channel width of 1 mm and channel length of 100 μm, respectively. For the deposition of interdigitated electrode, a commercial tungsten mask with channel width of 18 mm and channel length of 50 μm was used (channel area is 0.9 mm^2, Figure 5a). By connecting four interdigitated electrodes in parallel, the total light detecting area was increased to 3.6 mm^2 (right side of Figure 5a). For comparison, regular C8-BTBT phototransistors were also fabricated with same channel length (50 μm) and short channel width (1 mm) which gave a device area of 0.05 mm^2. The electrical characteristics of these devices were measured in ambient conditions with two computer-controlled Keithley 2400 source meters.

Optical Absorption Measurement: During the polarized absorption spectrum measurements, the C8-BTBT:PS films were spin coated on PVP:HDA covered quartz. The measurement was carried out with a UV–vis spectrophotometer (Thermo Scientific, Evolution 201) combined with a polarizer. The light spot was a narrow rectangle with a size of 1–3 mm.

Light Detecting: The UV light was generated from a commercial deep UV light emitting diodes with a wavelength of 354 nm (Sensor Electronic Technology, Inc.). The UV intensity was controlled by using neutral filters and changing the driving current. During the light detection process, the photodetector and UV LED was placed in a metal box to exclude the influence by ambient light. In the measurement of the response spectrum, a sunlight simulator combined with a computer-controlled monochromator was used for the generation of monochromatic light with a wavelength ranging from 250 to 1100 nm. The incident monochromatic light was changed to linear polarized light by locating a polarizer in the optical path. The intensity of the incident light at different wavelength was calibrated by a commercial Si photodetector.

Supporting Information

Supporting Information is available from the Wiley Online Library or from the author.

Acknowledgements

The authors thank financial support by the Academic Research Initiative at Domestic Nuclear Detection Office, U.S. Department of Homeland Security under award 2014-DN-077-ARI069-02 and National Science Foundation under award ECCS-1348272.

Received: October 5, 2015
Revised: October 14, 2015
Published online: November 17, 2015

[1] C. W. Tang, S. VanSlyke, *Appl. Phys. Lett.* **1987**, *51*, 913.
[2] G. Li, V. Shrotriya, J. Huang, Y. Yao, T. Moriarty, K. Emery, Y. Yang, *Nat. Mater.* **2005**, *4*, 864.
[3] a) Z. Bao, J. Locklin, *Organic Field Effect Transistors*, CRC Press, Boca Raton, FL **2007**; b) G. H. Gelinck, H. E. A. Huitema, E. van Veenendaal, E. Cantatore, L. Schrijnemakers, J. B. van der Putten, T. C. Geuns, M. Beenhakkers, J. B. Giesbers, B.-H. Huisman, *Nat. Mater.* **2004**, *3*, 106; c) H. Sirringhaus, T. Kawase, R. Friend, T. Shimoda, M. Inbasekaran, W. Wu, E. Woo, *Science* **2000**, *290*, 2123.
[4] a) N. G. Woodard, E. G. Hufstedler, G. P. Lafyatis, *Appl. Phys. Lett.* **1994**, *64*, 1177; b) K. K. E. Committee, *Hamamatsu PMT Handbook*, Hamamatsu Photonics, **2006**.

[5] Y. Matsumura, H. N. Ananthaswamy, *Toxicol. Appl. Pharm.* **2004**, *195*, 298.
[6] D. Decoster, J. Harari, *Optoelectronic Sensors*, John Wiley & Sons, London **2013**.
[7] J. Artiola, I. L. Pepper, M. L. Brusseau, *Environmental Monitoring and Characterization*, Academic Press, San Diego, CA **2004**.
[8] M. Razeghi, A. Rogalski, *J. Appl. Phys.* **1996**, *79*, 7433.
[9] a) P. Schreiber, T. Dang, T. Pickenpaugh, G. A. Smith, P. Gehred, C. W. Litton, presented at Proc. SPIE 3629, Photodetectors: Materials and Devices, San Jose, CA, April **1999**; b) F. P. Neele, R. M. Schleijpen, presented at Proc. SPIE 5075, Targets and Backgrounds IX: Characterization and Representation, Bellingham, Washington, September **2003**.
[10] G. F. Knoll, *Radiation Detection and Measurement*, John Wiley & Sons, Michigan **2010**.
[11] H. Iams, B. Salzberg, *Proc. IEEE* **1935**, *23*, 55.
[12] Y. Yuan, Q. Dong, B. Yang, F. Guo, Q. Zhang, M. Han, J. Huang, *Sci. Rep.* **2013**, *3*, 2707.
[13] C. Soci, A. Zhang, B. Xiang, S. A. Dayeh, D. Aplin, J. Park, X. Bao, Y.-H. Lo, D. Wang, *Nano Lett.* **2007**, *7*, 1003.
[14] a) R. Dong, Y. Fang, J. Chae, J. Dai, Z. Xiao, Q. Dong, Y. Yuan, A. Centrone, X. C. Zeng, J. Huang, *Adv. Mater.* **2015**, *27*, 1912; b) Y. Fang, F. Guo, Z. Xiao, J. Huang, *Adv. Opt. Mater.* **2014**, *2*, 348; c) F. Guo, Z. Xiao, J. Huang, *Adv. Opt. Mater.* **2013**, *1*, 289; d) Y. Jin, J. Wang, B. Sun, J. C. Blakesley, N. C. Greenham, *Nano Lett.* **2008**, *8*, 1649.
[15] F. Guo, B. Yang, Y. Yuan, Z. Xiao, Q. Dong, Y. Bi, J. Huang, *Nat. Nanotech.* **2012**, *7*, 798.
[16] Y. Fang, J. Huang, *Adv. Mater.* **2015**, *27*, 2804.
[17] a) Y. Ma, C.-M. Che, H.-Y. Chao, X. Zhou, W.-H. Chan, J. Shen, *Adv. Mater.* **1999**, *11*, 852; b) H. Uoyama, K. Goushi, K. Shizu, H. Nomura, C. Adachi, *Nature* **2012**, *492*, 234; c) K. Takimiya, S. Shinamura, I. Osaka, E. Miyazaki, *Adv. Mater.* **2011**, *23*, 4347; d) C. D. Sheraw, T. N. Jackson, D. L. Eaton, J. E. Anthony, *Adv. Mater.* **2003**, *15*, 2009.
[18] a) B. J. de Gans, P. C. Duineveld, U. S. Schubert, *Adv. Mater.* **2004**, *16*, 203; b) R. Søndergaard, M. Hösel, D. Angmo, T. T. Larsen-Olsen, F. C. Krebs, *Mater. Today* **2012**, *15*, 36; c) F. C. Krebs, *Sol. Energ. Mat. Sol. Cells* **2009**, *93*, 394.
[19] a) J. Milvich, T. Zaki, M. Aghamohammadi, R. Rödel, U. Kraft, H. Klauk, J. N. Burghartz, *Org. Electron.* **2015**, *20*, 63; b) S.-T. Chuang, S.-C. Chien, F.-C. Chen, *Appl. Phys. Lett.* **2012**, *100*, 013309; c) B. Mukherjee, K. Sim, T. J. Shin, J. Lee, M. Mukherjee, M. Ree, S. Pyo, *J. Mater. Chem.* **2012**, *22*, 3192.
[20] E. H. Huisman, A. G. Shulga, P. J. Zomer, N. Tombros, D. Bartesaghi, S. Z. Bisri, M. A. Loi, L. J. A. Koster, B. J. van Wees, *ACS Appl. Mater. Interfaces* **2015**, *7*, 11083.
[21] Y. Yuan, G. Giri, A. L. Ayzner, A. P. Zoombelt, S. C. Mannsfeld, J. Chen, D. Nordlund, M. F. Toney, J. Huang, Z. Bao, *Nat. Commun.* **2014**, *5*, 3005.
[22] M. E. Roberts, N. Queraltó, S. C. Mannsfeld, B. N. Reinecke, W. Knoll, Z. Bao, *Chem. Mater.* **2009**, *21*, 2292.
[23] M. Salinas, C. M. Jäger, A. Y. Amin, P. O. Dral, T. Meyer-Friedrichsen, A. Hirsch, T. Clark, M. Halik, *J. Am. Chem. Soc.* **2012**, *134*, 12648.
[24] H. Minemawari, T. Yamada, H. Matsui, J. y. Tsutsumi, S. Haas, R. Chiba, R. Kumai, T. Hasegawa, *Nature* **2011**, *475*, 364.
[25] M. Pope, C. E. Swenberg, *Electronic Processes in Organic Crystals and Polymers*, Vol. *74*, Oxford University Press, New York **1999**.
[26] K. J. Baeg, M. Binda, D. Natali, M. Caironi, Y. Y. Noh, *Adv. Mater.* **2013**, *25*, 4267.
[27] Y. Guo, C. Du, G. Yu, C. a. Di, S. Jiang, H. Xi, J. Zheng, S. Yan, C. Yu, W. Hu, *Adv. Funct. Mater.* **2010**, *20*, 1019.
[28] a) B. Yang, F. Guo, Y. Yuan, Z. Xiao, Y. Lu, Q. Dong, J. Huang, *Adv. Mater.* **2013**, *25*, 572; b) S. Kazaoui, R. Ross, N. Minami, *Phys. Rev. B* **1995**, *52*, R11665.
[29] C. Liu, T. Minari, X. Lu, A. Kumatani, K. Takimiya, K. Tsukagoshi, *Adv. Mater.* **2011**, *23*, 523.
[30] H.-S. Kang, C.-S. Choi, W.-Y. Choi, D.-H. Kim, K.-S. Seo, *Appl. Phys. Lett.* **2004**, *84*, 3780.
[31] a) H. Klauk, *Organic Electronics: Materials, Manufacturing, and Applications*, Wiley, Heisenbergstr **2006**; b) C. D. Dimitrakopoulos, P. R. Malenfant, *Adv. Mater.* **2002**, *14*, 99.
[32] a) H. Yu, Z. Bao, J. H. Oh, *Adv. Funct. Mater.* **2013**, *23*, 629; b) M. Y. Cho, S. J. Kim, Y. D. Han, D. H. Park, K. H. Kim, D. H. Choi, J. Joo, *Adv. Funct. Mater.* **2008**, *18*, 2905.
[33] a) M. Sofos, J. Goldberger, D. A. Stone, J. E. Allen, Q. Ma, D. J. Herman, W.-W. Tsai, L. J. Lauhon, S. I. Stupp, *Nat. Mater.* **2009**, *8*, 68; b) H.-Y. Chen, M. K. Lo, G. Yang, H. G. Monbouquette, Y. Yang, *Nat. Nanotech.* **2008**, *3*, 543; c) G. Konstantatos, E. H. Sargent, *Nat. Nanotech.* **2010**, *5*, 391; d) J.-S. Lee, M. V. Kovalenko, J. Huang, D. S. Chung, D. V. Talapin, *Nat. Nanotech.* **2011**, *6*, 348.
[34] J.-M. Liu, *Photonic Devices*, Cambridge University Press, Los Angeles **2005**.
[35] C. Tanase, E. Meijer, P. Blom, D. De Leeuw, *Phys. Rev. Lett.* **2003**, *91*, 216601.
[36] a) J. Smith, R. Hamilton, I. McCulloch, N. Stingelin-Stutzmann, M. Heeney, D. D. Bradley, T. D. Anthopoulos, *J. Mater. Chem.* **2010**, *20*, 2562; b) G. Horowitz, *J. Mater. Res.* **2004**, *19*, 1946.
[37] G. Konstantatos, M. Badioli, L. Gaudreau, J. Osmond, M. Bernechea, F. P. G. de Arquer, F. Gatti, F. H. Koppens, *Nat. Nanotech.* **2012**, *7*, 363.
[38] F. Hooge, T. Kleinpenning, L. Vandamme, *Rep. Prog. Phys.* **1981**, *44*, 479.
[39] J. Rhayem, M. Valenza, D. Rigaud, N. Szydlo, H. Lebrun, *J Appl. Phys.* **1998**, *83*, 3660.
[40] Y.-M. Lin, P. Avouris, *Nano Lett.* **2008**, *8*, 2119.